Neutral-Current Atmospheric Neutrino Flux Measurement Using Neutrino-Proton Elastic Scattering in Super-Kamiokande

John F. Beacom[1] and Sergio Palomares-Ruiz[1,2]
[1] *NASA/Fermilab Astrophysics Center, Fermi National Accelerator Laboratory, Batavia, Illinois 60510-0500, USA*
[2] *Departamento de Física Teórica, Universidad de Valencia, 46100 Burjassot, Valencia, Spain*
beacom@fnal.gov, Sergio.Palomares@uv.es
(Dated: January 9, 2003)

Recent results show that atmospheric ν_μ oscillate with $\delta m^2 \simeq 3 \times 10^{-3}$ eV^2 and $\sin^2 2\theta_{atm} \simeq 1$, and that conversion into ν_e is strongly disfavored. The Super-Kamiokande (SK) collaboration, using a combination of three techniques, reports that their data favor $\nu_\mu \to \nu_\tau$ over $\nu_\mu \to \nu_{sterile}$. This distinction is extremely important for both four-neutrino models and cosmology. We propose that neutrino-proton elastic scattering ($\nu + p \to \nu + p$) in water Čerenkov detectors can also distinguish between active and sterile oscillations. This was not previously recognized as a useful channel since only about 2% of struck protons are above the Čerenkov threshold. Nevertheless, in the present SK data there should be about 40 identifiable events. We show that these events have unique particle identification characteristics, point in the direction of the incoming neutrinos, and correspond to a narrow range of neutrino energies ($1 - 3$ GeV, oscillating near the horizon). This channel will be particularly important in Hyper-Kamiokande, with ~ 40 times higher rate. Our results have other important applications. First, for a similarly small fraction of atmospheric neutrino quasielastic events, the proton is relativistic. This uniquely selects ν_μ (not $\bar{\nu}_\mu$) events, useful for understanding matter effects, and allows determination of the neutrino energy and direction, useful for the L/E dependence of oscillations. Second, using accelerator neutrinos, both elastic and quasielastic events with relativistic protons can be seen in the K2K 1-kton near detector and MiniBooNE.

PACS numbers: 13.15.+g, 25.30.Pt, 29.40.Ka FERMILAB-Pub-03/003-A, FTUV-03-0109, IFIC/03-01

I. INTRODUCTION

High-statistics atmospheric neutrino data from Super-Kamiokande (SK) show ν_μ vacuum oscillation disappearance with $\delta m^2 \simeq 3 \times 10^{-3}$ eV^2 and $\sin^2 2\theta_{atm} \simeq 1$ [1]. Both atmospheric [1] and reactor [2] data strongly disfavor $\nu_\mu \to \nu_e$ oscillations, so one of the crucial remaining questions is whether the oscillations are of $\nu_\mu \to \nu_\tau$ or $\nu_\mu \to \nu_{sterile}$, or a mixture. A definite answer would have important implications for four-neutrino mixing models designed to accommodate [3] the LSND signal [4] and also for the role of neutrinos in cosmology [5].

A variety of techniques have been proposed to distinguish between atmospheric $\nu_\mu \to \nu_\tau$ and $\nu_\mu \to \nu_{sterile}$ oscillations [6, 7, 8, 9, 10]. The SK collaboration reports that their data favor pure active oscillations $\nu_\mu \to \nu_\tau$ over pure sterile oscillations $\nu_\mu \to \nu_{sterile}$ at better than the 99% CL [11], though an appreciable sterile admixture remains possible. This claim is based on a combination of three techniques: (i) matter effects on the partially-contained and throughgoing-muon samples, (ii) the contribution of inelastic neutral-current events with pions to the fully-contained multi-ring events sample, and (iii) statistically-identified tau lepton decays. Individually, these techniques do not offer strong evidence, and the latter two are made difficult by large backgrounds.

We propose a new technique for active-sterile discrimination: neutrino-proton elastic scattering,

$$\nu + p \to \nu + p\,, \tag{1.1}$$

from both free and bound protons, where the struck proton is above the Čerenkov threshold (see also a related detection application at low energies in Ref. [12]). This is a neutral-current (NC) channel, and so directly measures the total active neutrino flux. The number of charged-current (CC) atmospheric neutrino events in SK is $\sim 10^4$, and the ratio of cross sections $\sigma_{NC}/\sigma_{CC} \simeq 0.2$ for both neutrinos and antineutrinos in this energy range [13], so we expect $\sim 10^3$ NC events. It has always been assumed that protons above the Čerenkov threshold are too small in number and too difficult to identify. We show that the number of events is reasonable and that the protons are identifiable. The protons are directional, and an up-down ratio discriminates between active and sterile oscillations since upgoing ν_τ are fully detectable while upgoing $\nu_{sterile}$ are invisible.

This detection channel for atmospheric neutrinos in SK was mentioned by Vissani and Smirnov, but was dismissed as having too few events above the Čerenkov threshold [6]. Some estimates for the event rate were mentioned in SK Ph.D. theses [14]. In those studies, all of the protons were classified by the Monte Carlo as either e-like or μ-like, and were assumed to be buried by the much more numerous relativistic electrons and muons from CC channels. It is unknown what fraction of relativistic protons failed general cuts designed for electrons and muons, and hence were not classified at all.

In what follows, we develop the case that atmospheric neutrino-proton elastic scattering events above the Čerenkov threshold should be in the present SK data set, that they can be identified, and that they will be very useful in studying neutrino oscillations. Finally, we identify some other applications of our results.

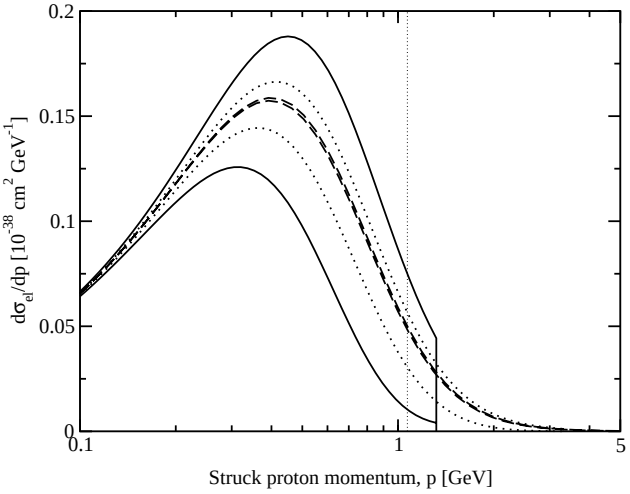

FIG. 1: Differential $\nu + p \to \nu + p$ cross section as a function of proton momentum (note log scale used for display). Upper lines correspond to neutrinos and lower lines to antineutrinos, at $E_\nu = 1$ GeV (solid), 3 GeV (dotted), and 50 GeV (dashed), terminated at the maximum allowed proton momentum (only visible in the 1 GeV case). The Čerenkov threshold in water at $p = 1.07$ GeV is shown with a thin dotted line.

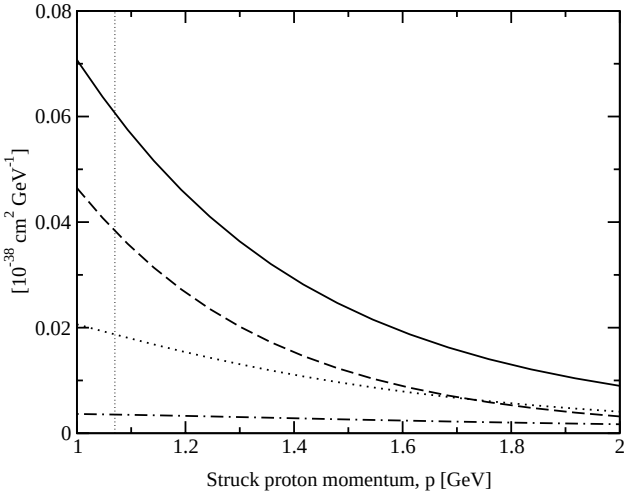

FIG. 2: The components of the differential $\nu + p \to \nu + p$ cross section: the sum (solid line), A term (dot-dashed line), B term (dotted line) and C term (dashed line) for $E_\nu = 2$ GeV, as a function of the recoil proton momentum p. For antineutrinos, the B term contributes with the opposite sign, and so the differential cross section is much smaller. Note that only $p > 1$ GeV is shown, in contrast to Fig. 1.

II. CROSS SECTION FOR $\nu + p \to \nu + p$

A. Free Proton Targets

The neutrino-proton elastic scattering cross section is an important prediction of the Standard Model that has been confirmed at GeV energies, e.g., in the E734 experiment [13]. The differential cross section on free proton targets in terms of the struck proton momentum p (and corresponding mass M_p, kinetic energy T_p, and total energy E_p) and neutrino energy E_ν is given by [15]

$$\frac{d\sigma_{el}}{dp} = \frac{G_F^2 M_p^3 p}{4\pi E_\nu^2 E_p}\left[A \mp B\frac{(s-u)}{M_p^2} + C\frac{(s-u)^2}{M_p^4}\right] . \quad (2.1)$$

The minus (plus) is for neutrinos (antineutrinos), and

$$\begin{aligned} A &= 4\tau\left[G_A^2(1+\tau) - F_1^2(1-\tau)\right. \\ &+ \left. F_2^2(1-\tau)\tau + 4F_1F_2\tau\right] \quad (2.2)\\ B &= 4\tau G_A(F_1+F_2) \quad (2.3)\\ C &= \frac{1}{4}\left(G_A^2 + F_1^2 + F_2^2\tau\right) , \quad (2.4) \end{aligned}$$

where $s - u = 4M_p\,(E_\nu - M_p\tau)$, $\tau = Q^2/4M_p^2$, and $Q^2 = -q^2 = 2M_pT_p$. The differential cross section is shown in Fig. 1. Almost all of the struck protons are below the Čerenkov threshold; the subject of this paper are those few above it. Since this is a neutral-current channel, all active flavors of neutrinos contribute equally (though the antineutrino cross section is smaller at the relevant E_ν). We consider backgrounds to the detection of protons in the elastic channel in detail below.

The most important proton recoil momenta lie between about 1 and 2 GeV. The lower limit is determined by the Čerenkov threshold in water at 1.07 GeV, and the upper limit by the falling differential cross section (and neutrino spectrum). In Fig. 2, we show the separate terms of the differential cross section for $E_\nu = 2$ GeV (other relevant energies give similar results). The most important terms in Eq. (2.1) are the B and C terms, which are comparable. For neutrinos, they add constructively, and for antineutrinos, they add destructively. The suppression of the differential cross section at large proton momenta is caused by the decrease of the form factors at large Q^2.

The vector form factors F_1 and F_2 that couple the exchanged Z° to the proton have been well measured in electron-nucleon scattering, and are

$$\begin{aligned} F_1 &= (1 - 2\sin^2\theta_W)(G_V^3 - F_V^3)\\ &- \frac{2}{3}\sin^2\theta_W(G_V^0 - F_V^0) \quad (2.5)\\ F_2 &= (1 - 2\sin^2\theta_W)F_V^3 - \frac{2}{3}\sin^2\theta_W F_V^0 , \quad (2.6) \end{aligned}$$

where $\sin^2\theta_W = 0.231$. The remaining form factors have a dipole form (vector mass $M_V = 0.84$ GeV), and are

$$\begin{aligned} G_V^3 &= \frac{1}{2}\frac{1 + \kappa_p - \kappa_n}{(1 + Q^2/M_V^2)^2} \quad (2.7)\\ G_V^0 &= \frac{3}{2}\frac{1 + \kappa_p + \kappa_n}{(1 + Q^2/M_V^2)^2} \quad (2.8)\\ F_V^3 &= \frac{1}{2}\frac{\kappa_p - \kappa_n}{(1+\tau)(1 + Q^2/M_V^2)^2} \quad (2.9)\\ F_V^0 &= \frac{3}{2}\frac{\kappa_p + \kappa_n}{(1+\tau)(1 + Q^2/M_V^2)^2} , \quad (2.10) \end{aligned}$$

where $\kappa_p = 1.793$ and $\kappa_n = -1.913$ are the proton and neutron anomalous magnetic moments.

The axial form factor is assumed to have a dipole form (axial mass $M_A = 1.03$ GeV), given by

$$G_A = -\frac{1}{2}\frac{1.267}{(1+Q^2/M_A^2)^2}\,. \qquad (2.11)$$

The main uncertainty in the differential cross section, Eq. (2.1), is caused by uncertainties in G_A. While neutrino scattering experiments suggest $M_A = 1.03$ GeV, charged-pion electroproduction data [16] suggest $M_A = 1.08$ GeV; all of the data are reviewed in Ref. [17]. The larger value of M_A would increase the differential cross section by about 10% in the interval we are interested in. There can also be strange sea quark contributions to all of the form factors, especially the spin contribution Δs that modifies the axial form factor [18], possibly increasing the differential cross section by about 10%. However, the effects of changing Δs and M_A are correlated. We do not assume enhancements to the cross section from either a larger M_A or a Δs contribution.

B. Nuclear Effects

We have so far only considered free protons, which are 2 out of 10 targets in water. Bound protons have nonzero initial momenta (Fermi motion), and the struck protons cannot make transitions to already-filled states at low energies (Pauli blocking). In typical Fermi-gas models ($p_F \simeq 220$ MeV) for neutrino interactions at a few GeV, these effects reduce the total cross section by about 20% [19]. However, these effects can be neglected when the struck proton is above the Čerenkov threshold. In this limit, the struck proton is ejected from the nucleus and the momentum transfer greatly exceeds the initial momentum. This may be seen from the differential cross section results (for the CC channel) in Refs. [19, 20].

The struck proton may reinteract as it leaves the nucleus [20]; at the relevant momenta, the interaction probability is about 1/2, corresponding mostly to forward elastic collisions [21]. There are neutrino interaction codes [22] that take nuclear reinteractions into account, but we do not. The average momentum loss for protons bound in oxygen in quasielastic scattering using the K2K neutrino beam is only $\simeq 90$ MeV [21]; it is reasonable to assume a similar average value for elastic atmospheric neutrino events. Since the spectrum dN/dp is so steep (see below), taking this into account could reduce the number of events above the Čerenkov threshold by about 20%. We neglect this effect because we are also neglecting the fact that there would be some compensation to this loss from $\nu + n \to \nu + n$ (about 1.5 times larger than for protons) followed by a $n+p \to p+n$ nuclear reinteraction that transfers most of the momentum to the proton. A full detector Monte Carlo will be needed to model these effects, along with the details of the Čerenkov particle identification and backgrounds.

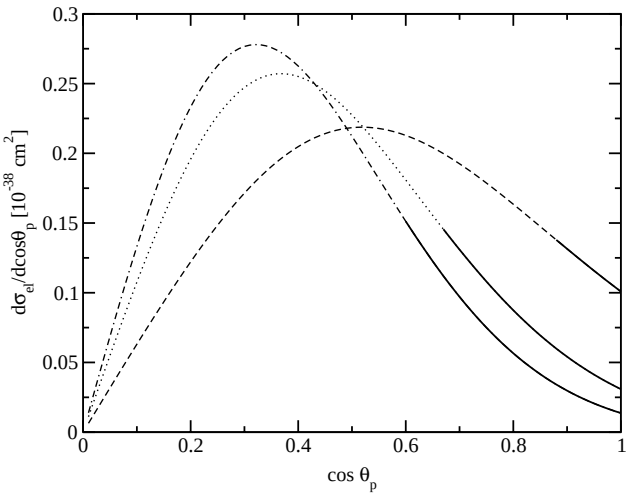

FIG. 3: The differential cross section $d\sigma_{el}/d\cos\theta_p$ (θ_p is the angle of the struck proton with respect to the incoming neutrino direction) for different neutrino energies, $E_\nu = 1$ (dashed line), 2 (dotted line), 3 GeV (dot-dashed line). The solid-line segment of each curve indicates protons that are above the Čerenkov threshold. Since we are neglecting proton reinteractions in the nucleus, only the forward hemisphere is shown.

C. Angular Distribution

In order to discriminate between active and sterile oscillations, the struck protons must be directional. The angles of the final particles relative to the initial neutrino direction are given by

$$\cos\theta_p = \frac{E_\nu + M_p}{E_\nu}\sqrt{\frac{T_p}{T_p + 2M_p}} \qquad (2.12)$$

$$\cos\theta_\nu = 1 - \frac{M_p T_p}{E_\nu(E_\nu - T_p)}\,. \qquad (2.13)$$

The maximum proton momentum is obtained when the neutrino reverses its direction and the proton goes forward. The most important neutrino energies for this channel are $1-3$ GeV, so for $\delta m^2 \simeq 3\times10^{-3}$ eV^2, the oscillation length corresponds to the direction of the horizon. Thus downgoing ν_μ have not oscillated yet, and upgoing ν_μ have oscillated into either ν_τ (same rate as downgoing) or $\nu_{sterile}$ (a reduced rate). As shown in Fig. 3, most protons emerge at rather large angles relative to the neutrino direction. However, these are the same majority of protons that are below the Čerenkov threshold. The relevant protons above the Čerenkov threshold are in fact quite forward, but not perfectly so (we show below that the lowest neutrino energies are the most relevant). Compared to the intrinsic angular variation, angular deflections from nuclear reinteractions [21] can almost always be ignored.

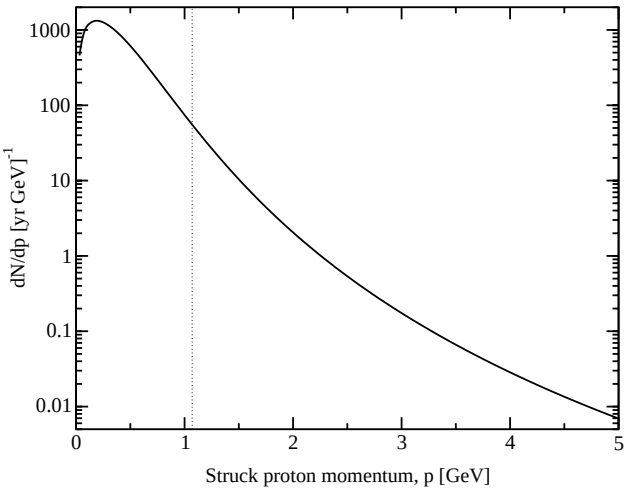

FIG. 4: Proton spectrum, dN/dp (yr GeV)$^{-1}$, as a function of proton momentum (solid line) in the 22.5 kton mass of SK. Note that the spectrum falls very quickly (vertical log scale). The Čerenkov threshold for protons in water is also shown (thin dotted vertical line).

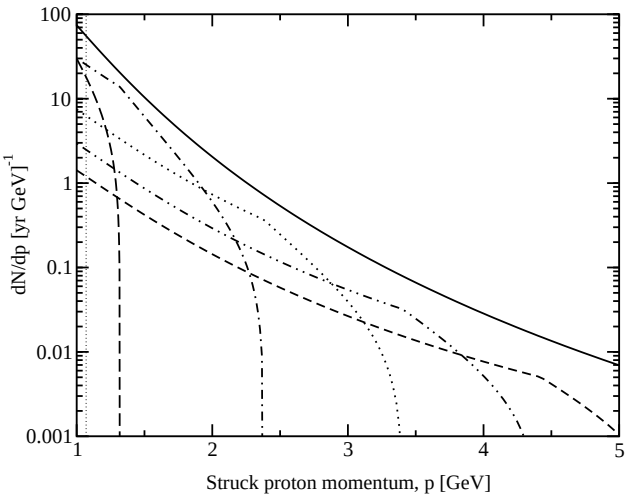

FIG. 5: Proton spectrum, dN/dp (yr GeV)$^{-1}$, as a function of proton momentum for different neutrino energy intervals contributing to it: all neutrinos (solid line), up to 1 GeV (dashed line), [1, 2] GeV (dot-dashed line), [2, 3] GeV (dotted line), [3, 4] GeV (doubly-dot-dashed line), [4, 5] GeV (short-dashed line). Note that only $p > 1$ GeV is shown.

III. PROTON RECOIL SPECTRUM

A. No-Oscillation Prediction

The struck proton momentum spectrum in SK for no oscillations (or oscillations among active flavors only) is

$$\frac{dN}{dp}(p) = Z \int_{(E_\nu)_{min}}^{\infty} dE_\nu \, \frac{dN_\nu}{dE_\nu}(E_\nu) \, \frac{d\sigma_{el}}{dp}(E_\nu, p) \qquad (3.1)$$

where $Z = 7.5 \times 10^{33}$ is the number of protons (free and bound) in the 22.5 kton fiducial mass of SK and $d\sigma_{el}/dp$ is the differential elastic cross section, Eq. (2.1). The atmospheric neutrino flux [23] dN_ν/dE_ν has been integrated over 4π (this is done only to calculate the total yields, as in practice the directionality of the protons can be used). We sum over all three flavors of neutrinos and antineutrinos, taking into account the reduced cross section for antineutrinos. The minimum neutrino energy for a given proton momentum is

$$(E_\nu)_{min} = \frac{1}{2}(E_p + p - M_p) \, . \qquad (3.2)$$

In Fig. 4, we show the complete momentum spectrum for protons elastically scattered by atmospheric neutrinos and antineutrinos in SK, per year of detector livetime.

The spectrum falls very steeply, and the fraction of protons above the Čerenkov threshold at $p = 1.07$ GeV is very small, about 2%. For the present exposure time of SK, 1489 days, we predict about 60 protons above the Čerenkov threshold (and about 2000 below). In order to normalize our results, we calculated the number of quasielastic events in SK; we agree with the SK no-oscillation numbers if we assume a detector efficiency of about 0.7 (approximately the official SK number). Thus in the present data there should be about 40 elastically-scattered protons above the Čerenkov threshold. This number is small, but it should be noted that much more data is expected from SK in the future. And indeed, possibly also from a future 1 Mton Hyper-Kamiokande detector with ~ 40 times higher rate [24] (or UNO, with ~ 20 times higher rate [25]); a high-statistics sample of neutrino-proton elastic scattering events could then be quickly collected.

The small number of protons above the Čerenkov threshold is a consequence of the large proton mass and the shape of the differential cross section, which falls steeply above a peak at $p \simeq 400$ MeV, as shown in Fig. 1. Additionally, the atmospheric neutrino spectrum is steeply falling with neutrino energy, and this is not compensated by growth in the cross section, since both the differential and total elastic cross sections become independent of neutrino energy above a few GeV.

About 95% of the protons above threshold are in the interval between $p = 1.07$ GeV and 2 GeV. This plays a crucial role in distinguishing protons from other charged particles, as well as the details of how they are stopped. In Fig. 5, we show how different ranges of neutrino energy contribute to the proton spectrum in this momentum interval. About 90% of the protons above the Čerenkov threshold are produced by neutrinos with $E_\nu < 5$ GeV, and in fact, the majority are produced by much lower neutrino energies. The kinks in Fig. 5 arise because we consider both minimum and a maximum neutrino energy to draw each curve; e.g., the dotted line for neutrino energies between 2 and 3 GeV has a kink at $p \simeq 2.4$ GeV because we do not include neutrino energies below 2 GeV.

B. Effect of Neutrino Oscillations

The vacuum oscillation length is

$$L_{osc} = \frac{4\pi E_\nu}{\delta m^2} \sim 1000 \left(\frac{E_\nu}{1\ \mathrm{GeV}}\right)\ \mathrm{km} \qquad (3.3)$$

where we have used $\delta m^2 \simeq 3 \times 10^{-3}\ \mathrm{eV}^2$ [1, 11]. This is close to the distance to the horizon, so that downgoing neutrinos have not oscillated and upgoing neutrinos have oscillated several times. Since the mixing is maximal, half of the upgoing ν_μ remain ν_μ and half oscillate to either ν_τ or $\nu_{sterile}$.

As shown in Fig. 3, the initial neutrino direction is largely maintained by the proton direction, the latter to be measured from its Čerenkov cone. We show below that the neutrino energy can also be estimated from the proton Čerenkov information, so that L_ν/E_ν can be estimated on an event-by-event basis, which improves the ability to study neutrino oscillations. Even in the absence of a neutrino energy estimate, Fig. 5 shows that only a narrow range of neutrino energies contributes to the signal above the Čerenkov threshold but below where the proton spectrum is greatly diminished.

There are uncertainties in the neutrino-proton elastic scattering cross section, e.g., from the axial form factor as well as from nuclear corrections to the free-proton cross section. There are also uncertainties introduced by our simple modeling of SK. For example, the number of protons above the Čerenkov threshold is quite sensitive to the index of refraction; we assumed 1.33, but in a more careful treatment one would have to model the wavelength dependence of the Čerenkov emission, attenuation, index of refraction, and phototube quantum efficiency. Finally, there is also a 20% uncertainty on the atmospheric neutrino flux normalization. In light of these facts, we must focus on a normalization-independent observable such the zenith angle spectrum shape, or at least an up-down ratio.

Consider an initial atmospheric neutrino flavor ratio of $\nu_e : \nu_\mu : \nu_\tau = 1 : 2 : 0$, which is a good approximation. Downgoing neutrinos have not oscillated, and have these flavor ratios. However, the upgoing neutrinos have oscillated several times. For maximal mixing of ν_μ to either ν_τ or $\nu_{sterile}$, the flavor ratios for the upgoing events are either $1 : 1 : 1$ or $1 : 1 : 0$ (we ignore mixing with ν_e as well as matter effects). Since this is a neutral-current cross section, equally sensitive to all flavors, the upgoing flux divided by the downgoing flux would be 1 for pure active oscillations and 2/3 for pure sterile oscillations. Assuming 40 events in the present SK data, this corresponds to 20 downgoing events and either 20 (active case) or 13 (sterile case) upgoing events, the latter reflecting a 1.5 sigma deviation. Thus with the present data this technique could not be decisive, but none of the three techniques used by SK to distinguish ν_τ from $\nu_{sterile}$ is individually decisive [11]. The advantage of neutrino-proton elastic scattering is that it could be rather clean, both in concept and in practice.

IV. PROTON PARTICLE IDENTIFICATION

A. Electron and Muon PID

In this section, we show how relativistic protons from neutrino-proton elastic scattering can be separated from other single-ring events in a Čerenkov detector like SK. Quasielastic interactions of atmospheric neutrinos create relativistic electrons and muons that produce Čerenkov radiation, which is seen by phototubes as rings on the walls of the detector. The rates are large, of order 10^3 events per year, to be compared to of order 10 relativistic protons per year. However, the unique particle identification (PID) properties of protons will allow rejection of these backgrounds.

Electrons and muons are stopped by continuous electromagnetic energy losses (mostly ionization, but also radiative losses for electrons); Čerenkov radiation does not cause significant energy loss. The continuous energy loss $-dE/dx$ is given by the Bethe-Bloch equation, reviewed in Ref. [26]. The range of a charged particle, the distance required to bring it to rest, is obtained immediately by integration. In Fig. 6, we show the range of muons in water as a function of momentum. Electrons, because of their small mass, have higher $-dE/dx$ for the same momentum and are stopped in less distance; in addition, multiple scattering changes their direction. We also show a range curve for protons, which would be correct if protons only lost energy electromagnetically (at high momenta, where $\beta = 1$, the proton and muon range are nearly the same; at low momenta, the proton velocity is less and hence the electromagnetic losses are higher). However, for protons in the relevant momentum range, discrete nuclear collisions are more important than continuous electromagnetic energy losses.

Since most atmospheric neutrinos are at energies of at least a GeV, the electrons and muons created in quasielastic reactions almost all have an initial velocity of $\beta \simeq 1$. This corresponds to the maximum Čerenkov intensity, and a Čerenkov emission angle of 41° in water. For muons, the outer edge of the Čerenkov rings is sharp, but for electrons, which suffer changes in direction due to multiple scattering, the outer edge has a more fuzzy appearance. As the velocity decreases, the Čerenkov angle and intensity both decrease. In an ideal detector, the rings on the wall would fill in completely as the particle slowed down (and approached the wall). In practice, the rapid decrease in the Čerenkov angle and intensity once the particle falls below $\beta \simeq 1$ mean that the inner edge of the Čerenkov rings is typically undersampled. This is especially true for electrons, which lose velocity in less distance than muons. Thus muon rings have a sharp outer edge and are partially filled in, whereas electron rings are fuzzy and not filled in. Electrons and muons can be very reliably distinguished in SK (to about 1%), as has been confirmed by a variety of means, including direct beam tests at KEK [27].

B. Proton PID: Nuclear Collisions Only

Unlike electrons and muons at these momenta, protons have a large cross section for nuclear collisions. If electromagnetic energy losses can be ignored, as we assume in this subsection, then the fraction of protons surviving a distance x without undergoing a nuclear collision is

$$N(x)/N(0) = \exp(-x/\lambda_N)\,. \tag{4.1}$$

For the nuclear attenuation length λ_N in water, we use

$$\lambda_N = [(\rho/M_{\rm H_2O})\ \sigma_{p+\rm H_2O}]^{-1}\ , \tag{4.2}$$

where $\rho/M_{\rm H_2O}$ is the number density of water molecules. For the cross section, we use

$$\sigma_{p+\rm H_2O} = \sigma_{p+^{16}\rm O} + 2\sigma_{p+p_{free}}\ . \tag{4.3}$$

Note that we cannot simply use the number density of nucleons in water, since nucleons bound in nuclei shadow each other (since nuclear densities are approximately constant, the cross sectional area of a nucleus scales as $A^{2/3}$). For scattering from ^{16}O, we use only the reaction (inelastic) cross section, taken from Ref. [28] (which corrects the earlier Ref. [29]). We have not included the elastic part of the cross section on ^{16}O, as it is very strongly peaked in the forward direction [30], corresponding to minimal momentum loss (for a proton with $p = 2$ GeV, a scattering angle less than 20 degrees corresponds to less than 1% change in momentum). For scattering from free protons, we do use the total cross section, taken from Ref. [26, 31]; since the target and projectile have the same mass, it is easier to have substantial momentum transfer. Above 1 GeV momentum, the proton nuclear cross section on water is nearly constant at about 390 mb; the oxygen reaction cross section is about 300 mb, and the proton cross section is about 45 mb.

In Fig. 6, we show the nuclear attenuation length for protons in water, ignoring electromagnetic losses. Above the Čerenkov threshold, this length is always shorter than the electromagnetic range of protons calculated if nuclear collisions are ignored. Thus in this subsection we consider that only nuclear collisions are important, and in the next subsection we calculate the corrections due to electromagnetic energy losses. In either case, protons have a short path length and will be fully-contained events.

Since 95% of the proton events are in the momentum range of $1-2$ GeV, with a steeply falling spectrum (see Fig. 5), a single nuclear collision with even moderate momentum transfer brings the proton below the Čerenkov threshold. In an inelastic collision with an oxygen nucleus that breaks it into several fragments, it is very unlikely than any of them are above the Čerenkov threshold. In a collision with a free proton, the initial momentum of less than 2 GeV is shared between both protons, leaving them both below the Čerenkov threshold (a forward elastic collision might exchange the projectile and target protons, causing little change in the Čerenkov pattern from no collision at all). Thus we assume that after a nuclear collision, there are no relativistic protons, neither the original proton nor any accelerated target protons.

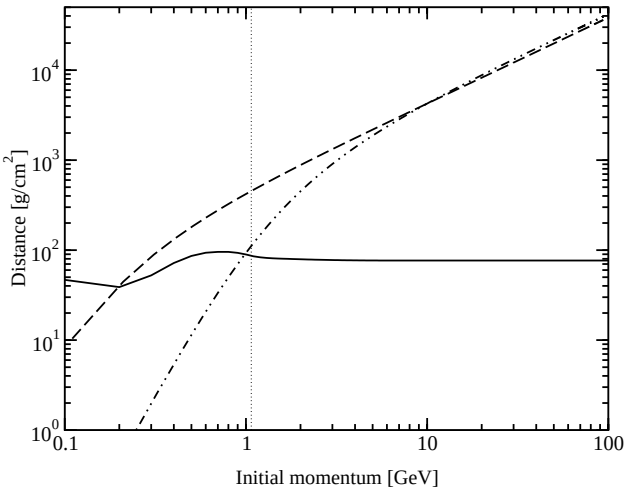

FIG. 6: Distance (g/cm^2) traveled in water by protons and muons as a function of momentum. We show the range (the distance to come completely to rest by electromagnetic losses alone) for muons (dashed line) and protons (dot-dashed line). For protons, we also show the nuclear attenuation length λ_N in water (solid line), the distance over which a fraction $1/e$ of protons travel without scattering. The Čerenkov threshold for protons is also shown (thin dotted vertical line).

Now we consider the Čerenkov signatures of the struck protons, assuming that a single nuclear collision brings the proton below the Čerenkov threshold. Protons have several unique PID characteristics. Since the proton velocity is constant until that collision, the Čerenkov angle and intensity are constant until they abruptly vanish. While the protons are relativistic, they do have $\beta < 1$, so their Čerenkov angle is less than the 41° for relativistic electrons and muons. Just as for muons, the outer edge of the Čerenkov rings is sharp for protons. However, since their Čerenkov angle is both smaller and constant, proton rings are filled in very densely and at a constant rate. The proton path length is rather short, of order $\lambda_N \simeq 80$ cm, compared to the several meters typical of muons, and thus the proton events are always fully contained. When the proton is abruptly stopped, the inner edge of the Čerenkov rings is also sharp, unlike for muons or electrons.

The number of Čerenkov photons produced per unit path length and photon wavelength interval by a particle of unit charge and velocity β is

$$\frac{d^2N_{ph}}{dx\,d\lambda} = \frac{2\pi\alpha}{\lambda^2}\ \left(1 - \frac{1}{\beta^2 n^2(\lambda)}\right) \tag{4.4}$$

In Fig. 7 we compare how the Čerenkov intensity and angle vary with the distance traveled for muons (electromagnetic losses only) and protons (nuclear collisions only). We choose the same initial velocities (and hence the same initial Čerenkov angle and intensity), using

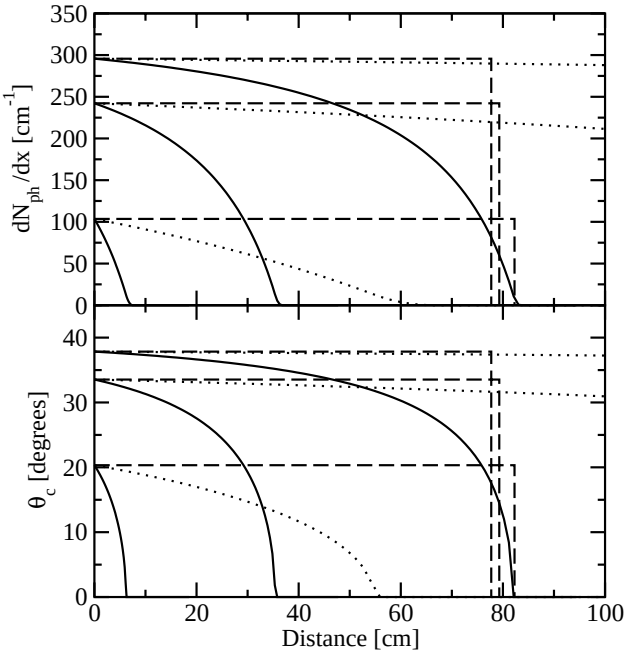

FIG. 7: Čerenkov intensity (upper plot) and angle (lower plot) as a function of the traveled path length in water for muons (solid lines) and protons, considering only nuclear collisions (dashed lines) or only electromagnetic losses (dotted lines). From bottom to top, the initial velocities are $\beta = 0.8$, 0.9, and 0.95. The Čerenkov intensity is calculated for visible light, without attenuation or detection efficiency. With electromagnetic losses neglected, individual protons always stop abruptly, but with a distribution of path lengths, Eq. (4.1); we used the average path length λ_N in the figure.

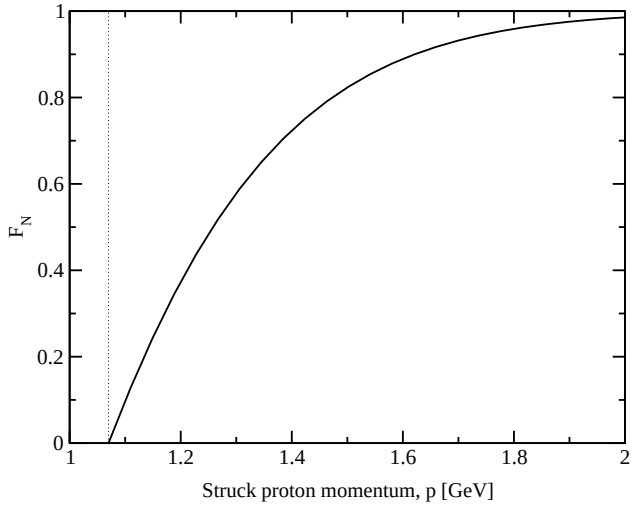

FIG. 8: The fraction of protons that go below the Čerenkov threshold by a nuclear collision as a function of proton momentum. The Čerenkov threshold for protons in water is also shown (thin dotted vertical line)

$\beta = 0.8$, 0.9, and 0.95, to highlight how the muon and proton stopping mechanisms differ. These correspond to muon momenta of 140 MeV, 220 MeV, and 320 MeV; and to proton momenta of 1.25 GeV, 1.95 GeV, and 2.85 GeV. Muons of a given β travel a well-defined distance before they fall below the Čerenkov threshold. However, protons of a given β travel a variety of distances, sampled from the distribution in Eq. (4.1). In Fig. 7 we have adopted λ_N as the path length for protons, since this is the average value.

Most muons in the SK atmospheric neutrino data have much longer track lengths than shown here, and hence are distinguishable. Those muons shown in Fig. 7 have path lengths short enough to be confused with protons, but have very different Čerenkov characteristics. In addition, excepting the 20% of negative muons that capture on oxygen, fully contained muons can be tagged by their subsequent decay to an electron or positron of up to 53 MeV. Thus it should be possible to distinguish protons from muons with very high efficiency on an event-by-event basis. In some SK Ph.D. theses [14] the neutrino-proton elastic scattering cross section was included in the atmospheric neutrino Monte Carlo. Those events were automatically classified as e-like or μ-like and then considered to be buried by the much larger quasielastic event samples. Most were classified as μ-like, which is why we have emphasized distinguishing protons and muons. In fact, protons should be quite distinguishable from electrons as well.

Since the nuclear cross section is nearly constant, the proton track length is a poor estimator of the proton momentum, and event-by-event track length fluctuations from Eq. (4.1) are more important. However, the proton momentum can be reliably estimated by the constant Čerenkov angle and intensity, since those vary appreciably in the momentum range considered, where $\beta < 1$.

C. Proton PID: Inclusion of $-dE/dx$ Effects

From Fig. 6, it is clear that for protons with momentum somewhat above the Čerenkov threshold, electromagnetic losses can be neglected, as we have assumed. However, right at the Čerenkov threshold, this is no longer true, since the $-dE/dx$ losses are greater and the range is as small as the nuclear interaction length. Thus the proton behavior is different, as it is continuously slowing down. It may finally go below the Čerenkov threshold by either further electromagnetic losses or a nuclear collision. In Fig. 7, we show results for nuclear collisions only (dashed lines), as well as for electromagnetic losses only (dotted lines).

Since the nuclear interaction length is nearly independent of momentum, the fraction F_N of protons brought below the Čerenkov threshold by a single nuclear collision is:

$$F_N(p) \simeq 1 - e^{-r(p)/\overline{\lambda}_N} \tag{4.5}$$

where $r(p)$ is the distance a proton travels before going below the Čerenkov threshold, considering only electro-

magnetic losses, and $\overline{\lambda}_N = 80$ cm. Note $r(p)$ is not the full range, and a 1 GeV proton still travels about a meter, though invisibly. The fraction F_N is shown in Fig. 8. Lower-momentum protons are affected most by electromagnetic energy losses. Protons with $p \gtrsim 1.25$ GeV are more likely to be brought below Čerenkov threshold by a nuclear collision than by electromagnetic losses. In fact, if we convolve this curve with the falling spectrum of struck protons, Fig. 4, about half of all protons are brought below Čerenkov threshold by a nuclear collision.

For the protons brought below threshold by a nuclear collision, the discussion above about proton PID neglecting electromagnetic losses is the most appropriate, though in some cases there will be some slight decrease in the Čerenkov angle and intensity before they abruptly vanish. The remaining protons fall below the Čerenkov threshold more gradually, e.g., the lowest momentum case ($\beta = 0.8$) in Fig. 7, for which electromagnetic losses dominate. Nevertheless, the Čerenkov behavior is still quite different from muons. For muons at the same initial β, protons go much farther and produce much more Čerenkov light. For muons that travel the same distance above the Čerenkov threshold, the proton Čerenkov angle is much smaller and falls off more slowly with distance (the proton velocity is also less, leading to a higher Čerenkov ring density on the wall). Thus even low-momentum protons should be quite distinct from muons (and electrons). Finally, when electromagnetic losses dominate, the proton momentum can be estimated by conventional Čerenkov techniques.

D. Possible Complications

Since the number of neutrino-proton elastic scattering events above the Čerenkov threshold is small, of order 10 per year in SK, careful consideration of backgrounds will be necessary. Above, we have motivated the case that protons are distinguishable from the more numerous electrons and muons from the quasielastic channel; we now consider other possible backgrounds.

One possible background is from the quasielastic channel, $\nu_\mu + n \to \mu^- + p$, but with the muon below the Čerenkov threshold and the proton above it. However, the total number of quasielastic events with a sub-Čerenkov muon is very low, about 35 per year in SK [32]. Most of these are produced by low-energy neutrinos; for high-energy neutrinos, the fraction with a relativistic proton is only about 2%. Thus this background is negligible.

There are also neutrino-neutron elastic scattering events (in fact, the cross section is about 1.5 times larger than for protons) in which the struck neutron carries a large momentum. Such events are of course invisible in SK. However, the struck neutrons can sometimes scatter a proton with enough momentum transfer that the proton is above the Čerenkov threshold. In the E734 accelerator neutrino experiment, it was estimated that such events were about 15% of the measured neutrino-proton elastic scattering signal. It should be less here since that tracking calorimeter had a lower (sub-Čerenkov) threshold for protons. Note also that such events would partially compensate the loss of neutrino-proton elastic scattering events from nuclear reinteractions.

We ignore the production of pions, in the initial interaction, by proton reinteraction in the initial nucleus, or in the final nuclear collision. Pions produced in the initial interaction are not part of the neutrino-proton elastic scattering channel, and cause multi-ring events. We are only considering single-ring events. Neutral-current single-pion events with the pion absorbed in the nucleus could be a background to the elastic channel; however, the fraction of these events with a proton above the Čerenkov threshold should be even lower than 2%, due to kinematics. Monte Carlo and real data on on quasielastic scattering using accelerator neutrinos in the K2K SciFi detector suggest that secondary pion contributions are minimal [21]. In their Monte Carlo results, which have a much more complete treatment of the physics than we have presented here, the track multiplicity was always 1 (muon) or 2 (muon and proton), and never 3 (including secondary pions). Additionally, pions created in the final nuclear collision would be delayed from the initial proton by several nanoseconds. The figures in Ref. [21] also support our assumption that when a high-momentum proton has a nuclear collision, it suffers a large momentum loss without accelerating new protons.

Another possible source of background is atmospheric muons interacting with the surrounding rock and producing fast neutrons that can enter the detector without triggering the veto. These neutrons could in principle scatter protons above the Čerenkov threshold. Most neutrons are far too low in energy to be effective [33] and neutrons are strongly attenuated by the 4.5 m water shielding. Incidentally, neutrino-proton elastic scattering events might be visible in the Soudan-2 experiment [34], which has much less mass and shielding than SK but can detect lower-energy (sub-Čerenkov) protons in a tracking calorimeter. The number of events could be a few tens, but the neutron backgrounds could be comparable [6]. We are not aware of any official analysis of these events by the Soudan-2 collaboration. Fast neutrons from the walls can also produce neutral pions by nuclear collisions in the detector; if the two photon rings from the decay are overlapping, this can resemble an atmospheric ν_e event [35]. However, the SK collaboration has shown that such events contribute less than 0.1% of the atmospheric ν_e signal [36, 37].

In summary, a full Monte Carlo study will be needed to correctly implement the initial neutrino interactions, possible nuclear reinteractions, pions, nuclear stopping and electromagnetic losses, backgrounds, and most importantly the PID in a realistic detector. Nevertheless, we believe that it looks promising that the relatively few (of order 10 per year in SK) neutrino-proton elastic scattering events above the Čerenkov threshold can be detected with little background.

V. RELATED APPLICATIONS

A. Accelerator Neutrinos: NC and CC Channels

We are not aware of any experiments with $p = 1 - 2$ GeV proton beams in Čerenkov detectors that would test the PID techniques introduced above. However, it should be possible to use accelerator neutrino beams to initiate neutrino-proton elastic scattering events in the right momentum range. The spectrum of accelerator neutrinos does not extend as high in energy as for atmospheric neutrinos (though note Fig. 5 shows that most of the signal comes from low energy neutrinos), but the total numbers of events expected are much larger.

The K2K 1-kton near detector would be a good place to start, as this detector is designed to mimic SK [38]. This data could be very useful for developing proton PID techniques. It would also be useful to study quasielastic events in which the proton is above the Čerenkov threshold; these are about 8 times more numerous than the comparable elastic events (though $\sigma_{NC}/\sigma_{CC} \simeq 0.2$, the ratio of the differential cross sections for $p \simeq 1-2$ GeV is smaller). Measuring both the outgoing lepton and proton would allow reconstruction of the neutrino energy, useful for measuring the neutrino spectrum. With $\sim 10^5$ events expected, we estimate $\sim 10^3$ quasielastic and $\sim 10^2$ elastic events with a relativistic proton.

The MiniBooNE detector [39] could also be used. Since it is designed to test the LSND signal (small mixing angle and large δm^2) [4], it can be considered a near detector for oscillations with the atmospheric δm^2. It contains 0.68 ktons of mineral oil, and is primarily a Čerenkov detector (about 3:1 Čerenkov to scintillation light). MiniBooNE has unique characteristics that will help proton PID. The index of refraction in oil ($\simeq 1.5$) is larger than in water, allowing a lower Čerenkov threshold (and larger angle and intensity). The density of oil ($\simeq 0.8$ g/cm^3) is less than for water, which means longer tracks. And once a proton falls below the Čerenkov threshold, it still produces scintillation light. With $\sim 5 \times 10^5$ events expected, we estimate $\sim 5 \times 10^3$ quasielastic and $\sim 5 \times 10^2$ elastic events with a relativistic proton. These studies would be an appealing complement to plans to measure the elastic scattering cross section at $Q^2 = 0$, a test of the strange quark contribution Δs to the proton spin [40]. The combined elastic and quasielastic data could measure the Q^2-dependence of the uncertain axial form factor.

B. Atmospheric Neutrinos: CC Channel

As noted, we expect about 8 times more quasielastic than elastic events with a proton above the Čerenkov threshold. Thus we estimate about ~ 300 such events in the 1489-day SK data. Taking ν_μ oscillations into account would reduce this number since ν_μ oscillate to either ν_τ (mostly below the CC threshold) or $\nu_{sterile}$. This has a very important consequence from the point of view of atmospheric neutrino oscillations, as it would allow the determination of the neutrino energy and direction on an event-by-event basis, allowing a better measurement of the L/E dependence of oscillations. Note also that these quasielastic events with a proton are produced only by neutrinos, and not antineutrinos, useful to studying matter effects and the neutrino/antineutrino ratio [41].

VI. CONCLUSIONS

We propose that neutrino-proton elastic scattering, $\nu + p \to \nu + p$, could be a useful detection reaction for atmospheric neutrinos in SK. The fraction of protons above the Čerenkov threshold is not large, only about 2%, but there should be about 40 identifiable events in the present 1489-day data. We have shown that it should be possible to separate protons from electrons and muons, since the relevant protons are not fully relativistic and will typically be stopped by a single nuclear collision. Proton Čerenkov rings have sharp outer and inner edges, are very densely filled, and correspond to a short path length and small Čerenkov angle. These are fully-contained, single-ring events. In order to test our proposal, a detailed detector Monte Carlo simulation will be needed.

Neutrino-proton elastic scattering is a neutral-current reaction and so measures the total active neutrino flux. For the relevant neutrino energies, oscillations occur at the distance to the horizon. In addition, protons above the Čerenkov threshold preserve the neutrino direction. These facts mean that this data can be used to test atmospheric $\nu_\mu \to \nu_\tau$ versus $\nu_\mu \to \nu_{sterile}$ oscillations. Since there are normalization uncertainties in the atmospheric neutrino flux, the cross section, and aspects of the detection, an up-down asymmetry test should be used. Let us assume 40 identifiable events in the present SK data (no oscillations). With oscillations, there should be 20 downgoing events and either 20 ($\nu_\mu \to \nu_\tau$) or 13 ($\nu_\mu \to \nu_{sterile}$) upgoing events. While not decisive, other techniques for active-sterile discrimination are not individually decisive either; they obtain their power in combination. Neutrino-proton elastic scattering has the advantage of being clean in concept. The rate in the proposed Hyper-Kamiokande detector would be about 40 times larger [24].

Our results on neutrino-proton elastic scattering have other immediate and important applications. First, using accelerator neutrinos, this channel can be seen in the K2K 1-kton near detector and in MiniBooNE. This data will reduce the cross section uncertainties and develop the proton PID techniques. Tagging relativistic protons will be similarly useful in the quasielastic channel in these detectors. Second, for a small fraction of the atmospheric neutrino quasielastic events, the proton is relativistic and can be tagged using the techniques presented here. This uniquely selects ν_μ (not $\bar{\nu}_\mu$) events, useful for understanding matter effects, and allows determination of the neutrino energy and direction, useful for studying the L/E dependence of oscillations.

ACKNOWLEDGMENTS

We thank Steve Brice, Takaaki Kajita, Paolo Lipari, Mark Messier, Georg Raffelt, Michael Smy, Manuel Vicente-Vacas, and Sam Zeller for useful discussions. We are especially grateful to Mark Vagins for extensive discussions. JFB is supported as the David N. Schramm Fellow by Fermilab (operated by URA under DOE contract No. DE-AC02-76CH03000), and additionally by NASA under NAG5-10842. SPR is supported by the Spanish MCED with a graduate FPU fellowship, by the Spanish MCYT and FEDER European Funds through the project FPA2002-00612, and by the OCYT of the Generalitat Valenciana under the Grant GV01-94. SPR thanks the Fermilab Theoretical Astrophysics Group for hospitality.

[1] Y. Fukuda *et al.*, Phys. Lett. B **433**, 9 (1998); Y. Fukuda *et al.*, Phys. Lett. B **436**, 33 (1998); Y. Fukuda *et al.*, Phys. Lett. B **467**, 185 (1999); Y. Fukuda *et al.*, Phys. Rev. Lett. **82**, 2644 (1999).

[2] M. Apollonio *et al.*, Phys. Lett. B **466**, 415 (1999); F. Boehm *et al.*, Phys. Rev. D **64**, 112001 (2001).

[3] M. Maltoni, T. Schwetz, M. A. Tortola and J. W. Valle, Nucl. Phys. B **643**, 321 (2002); H. Pas, L. G. Song and T. J. Weiler, hep-ph/0209373; and references therein.

[4] A. Aguilar *et al.*, Phys. Rev. D **64**, 112007 (2001).

[5] P. Di Bari, Phys. Rev. D **65**, 043509 (2002); K. N. Abazajian, astro-ph/0205238; and references therein.

[6] F. Vissani and A. Y. Smirnov, Phys. Lett. B **432**, 376 (1998).

[7] Q. Y. Liu and A. Y. Smirnov, Nucl. Phys. B **524**, 505 (1998); R. Foot, R. R. Volkas and O. Yasuda, Phys. Rev. D **58**, 013006 (1998); P. Lipari and M. Lusignoli, Phys. Rev. D **58**, 073005 (1998). M. C. Gonzalez-Garcia, H. Nunokawa, O. L. Peres and J. W. Valle, Nucl. Phys. B **543**, 3 (1999); G. L. Fogli, E. Lisi and A. Marrone, Phys. Rev. D **63**, 053008 (2001).

[8] L. J. Hall and H. Murayama, Phys. Lett. B **436**, 323 (1998).

[9] L. J. Hall and H. Murayama, Phys. Lett. B **463**, 241 (1999); T. Stanev, Phys. Rev. Lett. **83**, 5427 (1999).

[10] S. Nussinov and R. Shrock, Phys. Rev. Lett. **86**, 2223 (2001); E. Kolbe, K. Langanke and P. Vogel, Phys. Rev. D **66**, 013007 (2002).

[11] S. Fukuda *et al.*, Phys. Rev. Lett. **85**, 3999 (2000); A. Habig, hep-ex/0106025.

[12] J. F. Beacom, W. M. Farr and P. Vogel, Phys. Rev. D **66**, 033001 (2002).

[13] L. A. Ahrens *et al.*, Phys. Rev. Lett. **56**, 1107 (1986) [Erratum-ibid. **56**, 1883 (1986)]; L. A. Ahrens *et al.*, Phys. Rev. D **35**, 785 (1987); L. A. Ahrens *et al.*, Phys. Lett. B **202**, 284 (1988).

[14] M. D. Messier, Ph. D. Thesis, UMI-99-23965; Jun Kameda, Ph. D. Thesis (2002); `http://www-sk.icrr.u-tokyo.ac.jp/sk/pub/`.

[15] C. H. Llewellyn Smith, Phys. Rept. **3**, 261 (1972).

[16] A. Liesenfeld *et al.*, Phys. Lett. B **468**, 20 (1999).

[17] V. Bernard, L. Elouadrhiri and U. G. Meissner, J. Phys. G **28**, R1 (2002).

[18] G. T. Garvey, W. C. Louis and D. H. White, Phys. Rev. C **48**, 761 (1993); W. M. Alberico, S. M. Bilenky and C. Maieron, Phys. Rept. **358**, 227 (2002); R. D. McKeown and M. J. Ramsey-Musolf, hep-ph/0203011.

[19] T. K. Gaisser and J. S. O'Connell, Phys. Rev. D **34**, 822 (1986).

[20] C. Bleve, G. Co, I. De Mitri, P. Bernardini, G. Mancarella, D. Martello and A. Surdo, Astropart. Phys. **16**, 145 (2001); G. Co', C. Bleve, I. De Mitri and D. Martello, Nucl. Phys. Proc. Suppl. **112**, 210 (2002).

[21] C. W. Walter, Nucl. Phys. Proc. Suppl. **112**, 140 (2002), `http://neutrino.kek.jp/nuint01/`.

[22] D. Casper, Nucl. Phys. Proc. Suppl. **112**, 161 (2002); Y. Hayato, Nucl. Phys. Proc. Suppl. **112**, 171 (2002); H. Gallagher, Nucl. Phys. Proc. Suppl. **112**, 188 (2002); `http://neutrino.kek.jp/nuint01/`.

[23] M. Honda, T. Kajita, K. Kasahara and S. Midorikawa, Phys. Rev. D **52**, 4985 (1995).

[24] Y. Itow *et al.*, hep-ex/0106019.

[25] C. K. Jung, hep-ex/0005046.

[26] K. Hagiwara *et al.*, Phys. Rev. D **66**, 010001 (2002).

[27] S. Kasuga *et al.*, Phys. Lett. B **374**, 238 (1996).

[28] R. E. Prael and M. B. Chadwick, Los Alamos National Laboratory Report LA-UR-97-1745 (May 6, 1997), `http://www-xdiv.lanl.gov/XCI/PEOPLE/rep/plist.html`.

[29] H. P. Wellisch and D. Axen, Phys. Rev. C **54**, 1329 (1996).

[30] D. F. Measday and C. Richard-Serre, CERN-69-17; H. Feshbach, *Theoretical Nuclear Physics: Nuclear Reactions* (John Wiley & Sons, Inc., New York, 1992).

[31] R. K. Tripathi, J. W. Wilson and F. A. Cucinotta, Nucl. Instrum. Meth. B **152**, 425 (1999).

[32] M. Malek *et al.*, hep-ex/0209028.

[33] F. Boehm *et al.*, Phys. Rev. D **62**, 092005 (2000); J. Wolf, hep-ex/0211032.

[34] W. W. Allison *et al.*, Phys. Lett. B **449**, 137 (1999).

[35] O. G. Ryazhskaya, JETP Lett. **60**, 617 (1994); O. G. Ryazhskaya, JETP Lett. **61**, 237 (1995).

[36] Y. Fukuda *et al.*, Phys. Lett. B **388**, 397 (1996).

[37] T. Kajita and Y. Totsuka, Rev. Mod. Phys. **73**, 85 (2001).

[38] M. H. Ahn *et al.*, hep-ex/0212007; Y. Oyama, hep-ex/0210030.

[39] E. Church *et al.*, "A proposal for an experiment to measure $\nu_\mu \to \nu_e$ oscillations and ν_μ disappearance at the Fermilab Booster: BooNE," FERMILAB-P-0898; I. Stancu *et al.*, "The MiniBooNE Detector Technical Design Report"; see `http://www-boone.fnal.gov/`.

[40] R. Tayloe, Nucl. Phys. Proc. Suppl. **105**, 62 (2002).

[41] M. C. Bañuls, G. Barenboim and J. Bernabéu, Phys. Lett. B **513**, 391 (2001); J. Bernabéu, S. Palomares-Ruiz, A. Pérez and S. T. Petcov, Phys. Lett. B **531**, 90 (2002); T. K. Gaisser and T. Stanev, astro-ph/0210512.